Electronic Supplementary Information (ESI) for:

Tuning calcium biosensors with a single-site mutation: Structural dynamics insights from femtosecond Raman spectroscopy

*Sean R. Tachibana, Longteng Tang, Yanli Wang, Liangdong Zhu, Weimin Liu, and Chong Fang**

Department of Chemistry, Oregon State University, Corvallis, Oregon 97331-4003, USA

Corresponding Author

*E-mail: Chong.Fang@oregonstate.edu. Phone: 541-737-6704.

TOC Page number

ESI Text

ESI Figures

ESI Tables

Additional **discussion** follows each figure caption and table footnote

ESI Text

Significance and Perspective

Fluorescent proteins and their derivatives are critically important in the bioimaging field and life sciences. The elucidation of the underlying conformational dynamics of a recently developed Ca^{2+} biosensor GEM-GECO1-P377R (Fig. 1a) involves transient Raman modes in the electronic excited state,[1,2] exhibiting distinct frequency and intensity evolution on the crucial femtosecond to picosecond timescales (Figs. 2–5) before the fluorescence events. As a result, we can mechanistically understand green fluorescence (i.e., biosensor functionality) in both the Ca^{2+}-free and bound state of the biosensor and how the pertaining excited state proton transfer (ESPT) reaction progresses on the intrinsic molecular timescales. In particular, we have implemented the emergent wavelength-tunable FSRS methodology to dissect the intricate H-bonding network (e.g., ESPT chain) around the chromophore,[3-6] in systematic comparison to other functional calcium biosensors studied by FSRS in our laboratory.[2,7,8] The comparative analysis and comprehension of crucial and multidimensional photochemical reaction coordinates about how the chromophore responds to light and transfers the proton forms *the structural dynamics basis* for the biosensor fluorescence, and in particular, the fluorescence modulation in response to Ca^{2+} binding. In contrast to more technically demanding time-resolved electron or X-ray diffraction to capture chemistry in action,[9] our line of inquiry on a table-top optical apparatus is filling a current knowledge gap (besides practical applications) in understanding the structural motions that power or accompany molecular fluorescence (i.e., an intrinsic ultrafast photochemical event). This work thus opens the door to targeted mutation(s) at strategic site(s) to achieve the desired biofunctions, transcending the boundaries of modern physical chemistry, biophysics and biochemistry, protein engineering, nonlinear optics, spectroscopy, and biological imaging.

ESI Figures

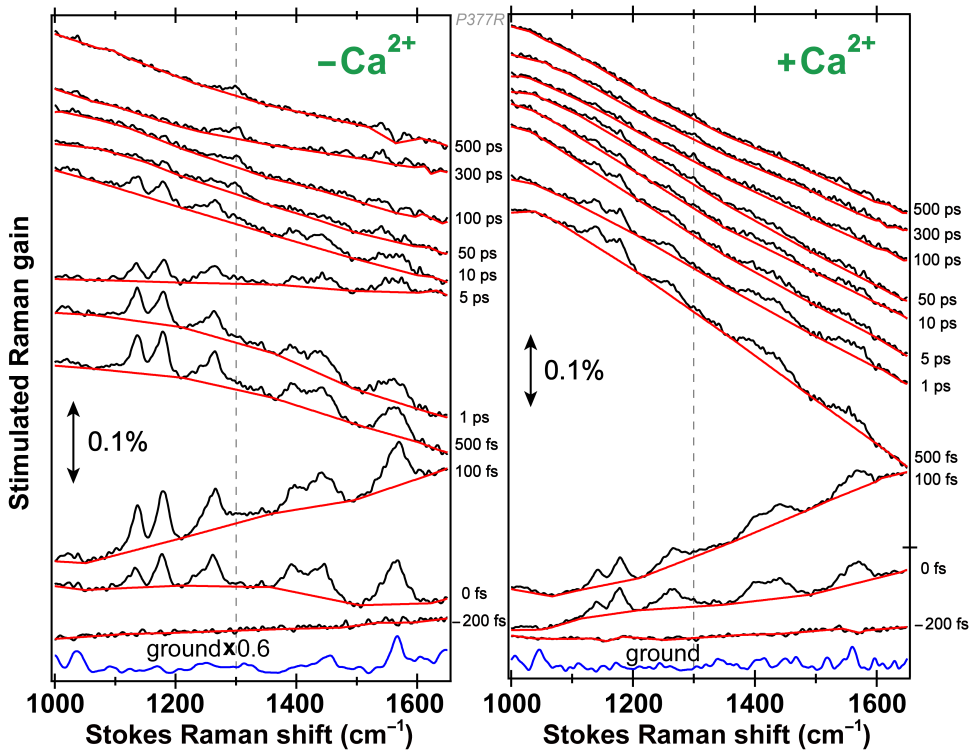

Fig. S1. Time-resolved excited state FSRS spectra of the Ca^{2+}-free (left) and Ca^{2+}-bound (right) GEM-GECO1-P377R biosensor with the spline baseline drawn for each time-delayed trace following 400 nm photoexcitation. Representative *raw experimental data* traces with evolving Raman peaks (black) are shown between –200 fs and 500 ps, while the baselines (red) are clearly broad and featureless. The double-arrowed vertical line denotes the stimulated Raman gain magnitude of 0.1%. The ground-state spectra (blue) are plotted at the bottom for comparison. The dashed lines highlight the emergence of transient I* peaks at ~1300 cm^{-1} on the ps timescale.

We note that the Raman peak intensity in the Ca^{2+}-bound biosensor is smaller than its Ca^{2+}-free counterpart, which may be due to some difference in sample concentration, laser power, resonance conditions,[10] electronic polarizability,[11] and photoexcitation pumping efficiency.[1,12] Therefore, instead of directly comparing peak intensities, we focus on analyzing the vibrational dynamics in each sample and retrieve the time constants to infer the effect of Ca^{2+} binding.

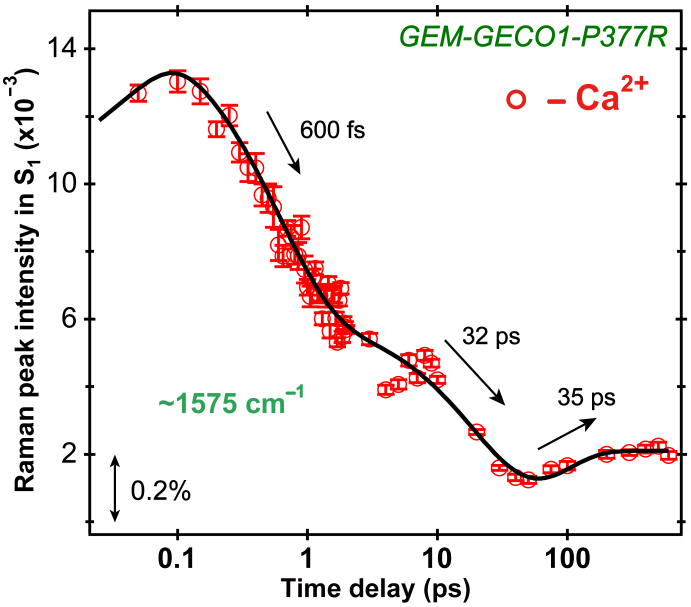

Fig. S2. Time-dependent integrated intensity of the ~1575 cm^{-1} mode in the Ca^{2+}-free P377R biosensor after 400 nm photoexcitation (an independent dataset to check the experimental reproducibility). The double-arrowed line indicates the stimulated Raman gain magnitude of 0.2%. The retrieved decay and rise time constants from the least-squares fit (black solid curve) are noted against the logarithmic time delay axis. The error bars (1 s.d.) are shown for all the time-dependent data points (red circles).

The initial 600 fs peak intensity decay is attributed to the protonated chromophore A* wavepackets moving out of the Franck-Condon region, which likely results in a rapid change of the resonance Raman conditions and the electronic polarizability change.[1,2] Because we least-squares fit the data trace from a common time zero, the 32 ps decay dynamics and the 35 ps rise dynamics can be associated with an ESPT reaction leading to the A* depletion and the concomitant deprotonated I* accumulation, respectively. These characteristic time constants match well with the ultrafast vibrational frequency dynamics shown in Fig. 3 (main text).

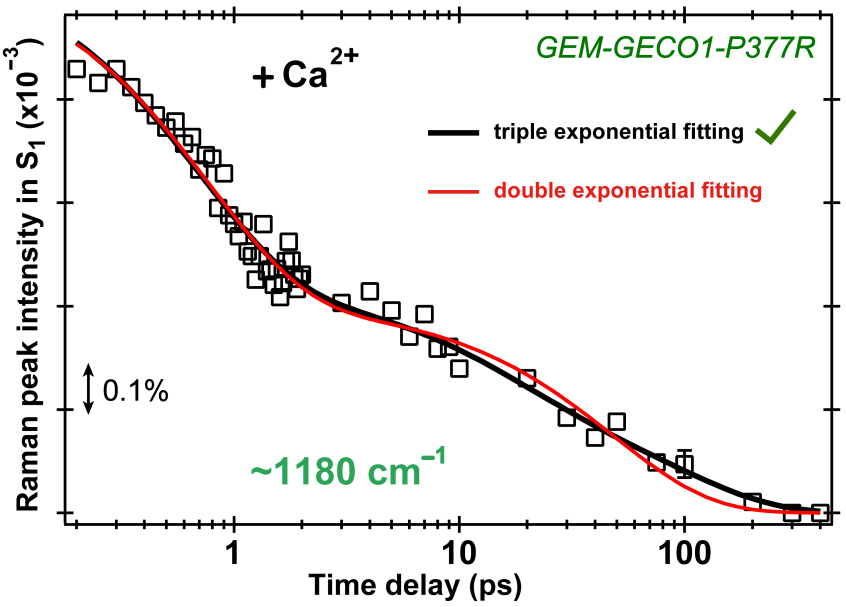

Fig. S3. Time-dependent integrated intensity of the ~1180 cm^{-1} mode in the Ca^{2+}-bound P377R biosensor after 400 nm photoexcitation. The data points (black squares) are overlaid with the triple-exponential (black solid curve) and double-exponential (red solid curve) least-squares fit from 200 fs to 400 ps (shown in logarithmic scales along the time axis). The double-arrowed line indicates the stimulated Raman gain magnitude of 0.1%. A representative error bar is shown at 100 ps time delay (with high signal-to-noise ratio), and the red curve is outside the error bar.

We select the 1180 cm^{-1} mode, one of the strongest Raman peaks in Figs. 2 and S1, to perform detailed analysis and to further minimize the effect of small uncertainties that could be associated with any kind of background subtraction method. The semi-logarithmic time-dependent peak intensity plot exhibits clear difference in the fit and the triple-exponential fit better matches the spectral data particularly for the later dynamics part beyond ~1 ps. This result is consistent with the largely conserved nature of initial A* structural dynamics that prepare the system for undergoing the ESPT reaction on the ps timescale, which in this case, consists of two pathways with the exponential time constants of 16 and 90 ps (see main text) to reach I*.

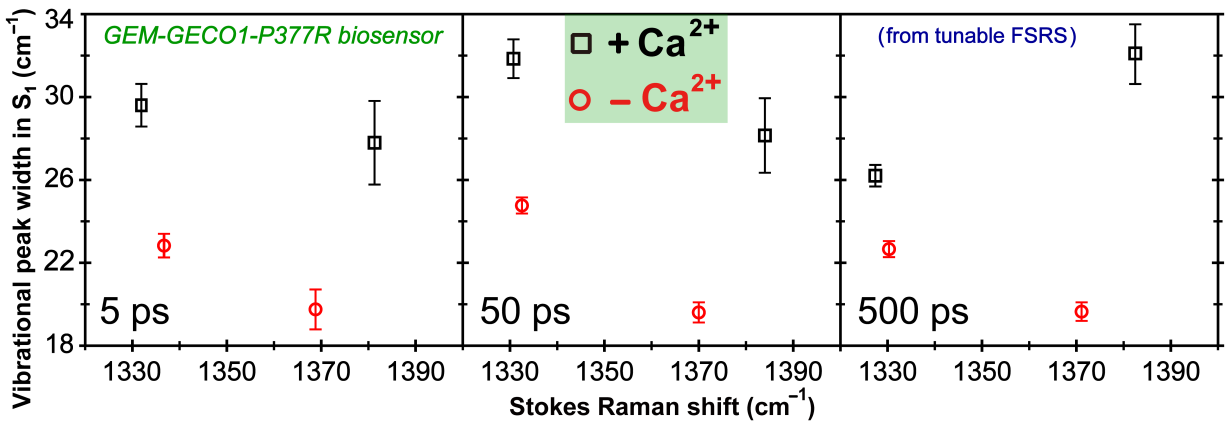

Fig. S4. Comparison of two excited state vibrational marker bands between the Ca^{2+}-free (red circles) and Ca^{2+}-bound (black squares) GEM-GECO1-P377R biosensors after 400 nm photoexcitation. The Raman pump is at 553 nm and the data points are selected from the time-resolved spectral traces in Fig. 4b. The representative time delay of 5, 50, and 500 ps is noted in each panel of the figure. The error bars (1 s.d.) for the least-squares fit peak widths (full width at half maximum of the Raman band, see the vertical axis) are shown. The horizontal axis records the Raman shift on the Stokes side in the spectral region of interest (in cm^{-1} unit).

Notably, the lower-frequency peak arises from a mixture of A* and I* modes as we observe the complex intensity dynamics starting from around the photoexcitation time zero in Fig. 4b. The associated peak width shows an interesting rise-drop pattern on the ps timescale as ESPT converts A* to I* species. In contrast, the higher-frequency mode emerges after ~2 ps and is likely attributed to an I* peak as a result of the ESPT reaction. In general, the Ca^{2+}-bound biosensor displays broader and further separated Raman peaks in this spectral region (ca. 1320—1400 cm^{-1}) than the Ca^{2+}-free biosensor (see main text for discussion and implications). The time-resolved peak frequency redshift and blueshift of the lower and higher frequency Raman band, respectively, is also notable in this figure (from the left to right panel).

ESI Tables

Table S1. Representative ground and excited state vibrational frequencies of P377R biosensor

	Expt. freq.[a] (cm^{-1})	Calc. freq.[b] (cm^{-1})	Major peak assignment
Ground state (S_0)	1567/1560	1571 (1552)	Phenolic ring C=C stretching and imidazolinone ring C=N stretching
Excited state (S_1)	1545 (1541) / 1543 (1537)	1511 (1502)	Phenolic COH rocking with phenolic ring C=C stretching, and imidazolinone ring C=N stretching
	1572 (1584) / 1571 (1582)	1587 (1619)	Phenolic ring C=C stretching and imidazolinone ring C=O stretching

[a] Observed Raman frequency of the ground and excited state peaks of P377R using an 800 nm Raman pump. In the excited state S_1 as mode frequency shift occurs (see Fig. 3), the average peak frequency from ca. 1—3 ps is followed by the average frequency from ca. 100—500 ps in parentheses. The Ca^{2+}-free and bound biosensor peak frequencies are separated by "/".

[b] The ground state calculations are performed using density functional theory (DFT) RB3LYP with 6-31G+(d,p) basis sets on the protonated and (deprotonated) chromophore *in vacuo* in Gaussian.[13] The excited state calculations are performed using the time-dependent DFT (TD-DFT) RB3LYP and the same basis sets (more related calculation results and comparisons can be found in our previous reports),[2,7,8,14] with the deprotonated chromophore results in parentheses. The frequency scaling factor is 0.96. Note that the observed frequency change matches the calculated redshift of the 1571 cm^{-1} mode in S_0 and 1511 cm^{-1} mode in S_1, as well as the blueshift of the 1587 cm^{-1} mode in S_1. This multi-mode correlation supports the assignment of the photochemical event revealed by FSRS (Figs. 2 and 4b) to the ESPT reaction which induces the chromophore deprotonation.

To assess the effect of ring twisting motion that makes the chromophore lose its two-ring coplanarity, we also perform a series of DFT calculations on the protonated chromophore in the electronic ground state.[8] The frequency scaling factor is 0.96. The phenolic ring C=C stretching and imidazolinone ring C=N stretching mode frequency redshifts from ~1571, 1569 to 1567 cm^{-1} as the dihedral angle around the bridge C=C bond (i.e., adjacent to the imidazolinone ring, see

Fig. 1b insert for the chromophore structure depiction) is fixed and varied from 0º, 20º to 40º. This trend is consistent with the observed redshift of the ~1545 cm^{-1} mode in S_1 (Fig. 3a), which suggests that ring twisting may accompany the ESPT reaction.[8,15,16]

Table S2. Mode assignment for the representative excited state vibrational peaks in tunable FSRS of the GEM-GECO1-P377R biosensor aided by quantum calculations

Expt. freq. (cm^{-1})[a]	Calc. freq. (cm^{-1})[b]	Major peak assignment
1267/1271	1286 (1289)	Phenolic C–O stretching, ring H rocking with asymmetric ring C=C stretching, and imidazolinone ring breathing
1336/1331	1343 (1348)	Bridge and phenol ring H out-of-phase rocking, imidazolinone ring C–N stretching
1370/1383	1393 (1390)	Phenolic C–O stretching, bridge C–C (close to phenol ring) stretching, bridge and phenol ring H in-phase rocking with imidazolinone ring C–N stretching

[a] Observed Raman frequency of the excited state peaks of the P377R biosensor using a 553 nm Raman pump. We average the peak frequencies from ca. 1—500 ps in Fig. 4b to highlight the I* contribution as a result of the chromophore deprotonation. The Ca^{2+}-free and bound biosensor peak frequencies are separated by "/".

[b] The excited state vibrational frequencies of a geometrically optimized protonated and (deprotonated) SYG chromophore are calculated using TD-DFT RB3LYP 6-31G+(d,p) *in vacuo* in Gaussian. The frequency scaling factor is 0.96. Tunable FSRS enhances the deprotonated chromophore more than the protonated chromophore,[8] and we expect that after photoexcitation, the transient A* features in Fig. 4b have partially deprotonated character prior to ~1 ps, followed by the I* species being accumulated on the ps timescale as a result of the ESPT reaction inside the biosensor protein pocket. The level of mismatch between the experimental and calculated peak frequency trend associated with chromophore deprotonation may arise from the incomplete modelling of inhomogeneous subpopulations which adopt non-uniform structural configurations.

ESI References

1 C. Fang, R. R. Frontiera, R. Tran and R. A. Mathies, *Nature*, 2009, **462**, 200-204.

2 B. G. Oscar, W. Liu, Y. Zhao, L. Tang, Y. Wang, R. E. Campbell and C. Fang, *Proc. Natl. Acad. Sci. U.S.A.*, 2014, **111**, 10191-10196.

3 M. Chattoraj, B. A. King, G. U. Bublitz and S. G. Boxer, *Proc. Natl. Acad. Sci. U.S.A.*, 1996, **93**, 8362-8367.

4 K. Brejc, T. K. Sixma, P. A. Kitts, S. R. Kain, R. Y. Tsien, M. Ormö and S. J. Remington, *Proc. Natl. Acad. Sci. U.S.A.*, 1997, **94**, 2306-2311.

5 S. R. Meech, *Chem. Soc. Rev.*, 2009, **38**, 2922-2934.

6 P. J. Tonge and S. R. Meech, *J. Photochem. Photobiol. A: Chemistry*, 2009, **205**, 1-11.

7 L. Tang, W. Liu, Y. Wang, Y. Zhao, B. G. Oscar, R. E. Campbell and C. Fang, *Chem. Eur. J.*, 2015, **21**, 6481-6490.

8 L. Tang, W. Liu, Y. Wang, L. Zhu, F. Han and C. Fang, *J. Phys. Chem. Lett.*, 2016, **7**, 1225-1230.

9 R. J. D. Miller, *Science*, 2014, **343**, 1108-1116.

10 A. B. Myers and R. A. Mathies, in *Biological Applications of Raman Spectroscopy*, ed. T. G. Spiro, John Wiley & Sons, Inc., New York, 1987, vol. 2, pp. 1-58.

11 J. L. McHale, *Molecular Spectroscopy*, Prentice-Hall, Upper Saddle River, NJ, 1999.

12 W. Liu, F. Han, C. Smith and C. Fang, *J. Phys. Chem. B*, 2012, **116**, 10535-10550.

13 M. J. Frisch, G. W. Trucks, H. B. Schlegel, G. E. Scuseria, M. A. Robb, J. R. Cheeseman, G. Scalmani, V. Barone, B. Mennucci, G. A. Petersson, H. Nakatsuji, M. Caricato, X. Li, H. P. Hratchian, A. F. Izmaylov, J. Bloino, G. Zheng, J. L. Sonnenberg, M. Hada, M. Ehara, K. Toyota, R. Fukuda, J. Hasegawa, M. Ishida, T. Nakajima, Y. Honda, O. Kitao, H. Nakai, T. Vreven, J. J. A. Montgomery, J. E. Peralta, F. Ogliaro, M. Bearpark, J. J. Heyd, E. Brothers, K. N. Kudin, V. N. Staroverov, R. Kobayashi, J. Normand, K. Raghavachari, A. Rendell, J. C. Burant, S. S. Iyengar, J. Tomasi, M. Cossi, N. Rega, J. M. Millam, M. Klene, J. E. Knox, J. B. Cross, V. Bakken, C. Adamo, J. Jaramillo, R. Gomperts, R. E. Stratmann, O. Yazyev, A. J. Austin, R. Cammi, C. Pomelli, J. W. Ochterski, R. L. Martin, K. Morokuma, V. G. Zakrzewski, G. A. Voth, P. Salvador, J. J. Dannenberg, S. Dapprich, A. D. Daniels, Ö. Farkas, J. B. Foresman, J. V. Ortiz, J. Cioslowski and D. J. Fox, *Gaussian 09, Revision B.1*, Gaussian, Inc., Wallingford, CT, 2009.

14 Y. Wang, L. Tang, W. Liu, Y. Zhao, B. G. Oscar, R. E. Campbell and C. Fang, *J. Phys. Chem. B*, 2015, **119**, 2204-2218.

15 N. Y. A. Baffour-Awuah and M. Zimmer, *Chem. Phys.*, 2004, **303**, 7-11.

16 S. Rafiq, B. K. Rajbongshi, N. N. Nair, P. Sen and G. Ramanathan, *J. Phys. Chem. A*, 2011, **115**, 13733-13742.